6-benzothiazolyl ureas, thioureas and guanidines are potent inhibitors of ABAD/17β-HSD10 and potential drugs for Alzheimer's disease treatment: Design, synthesis and *in vitro* evaluation

Ondrej Benek[1,2,3], Lukas Hroch[1,4], Laura Aitken[5], Rafael Dolezal[1,2], Patrick Guest[5], Marketa Benkova[1,6], Ondrej Soukup[1,3], Karel Musil[1,2], Rebecca Hughes[7] Kamil Kuca[1,2], Terry K Smith[7], Frank Gunn-Moore[5*], Kamil Musilek [1,2*]

[1]University Hospital in Hradec Kralove, Sokolska 581, 500 05 Hradec Kralove, Czech Republic

[2]University of Hradec Kralove, Faculty of Science, Department of Chemistry, Rokitanskeho 62, 500 03 Hradec Kralove, Czech Republic; kamil.musilek@gmail.com

[3]National Institute of Mental Health, Topolova 748, 250 67 Klecany, Czech Republic

[4]Charles University in Prague, Faculty of Pharmacy in Hradec Kralove, Department of Pharmaceutical Chemistry and Drug Control, Akademika Heyrovskeho 1203, 500 05Hradec Kralove

[5]University of St. Andrews, School of Biology, Medical and Biological Sciences Building, North Haugh, St. Andrews KY16 9TF, United Kingdom

[6]University of Defence, Faculty of Military Health Sciences, Department of Toxicology and Military Pharmacy, Department of Epidemiology, Trebesska 1575, 500 01 Hradec Kralove, Czech Republic

[7]Biomedical Science Research Complex, University of St. Andrews, North Haugh, St. Andrews. KY16 9ST, United Kingdom; fjg1@st-andrews.ac.uk

Abstract

Background: The mitochondrial enzyme amyloid beta-binding alcohol dehydrogenase (ABAD) also known as 17β-hydroxysteroid dehydrogenase type 10 (17β-HSD10) has been connected with the pathogenesis of Alzheimer's disease (AD). ABAD/ 17β-HSD10 is a binding site for the amyloid-beta peptide (Aβ) inside the mitochondrial matrix where it exacerbates Aβ toxicity. Interaction between these two proteins triggers a series of events leading to mitochondrial dysfunction as seen in AD. *Methods*: As ABAD's enzymatic activity is required for mediating Aβ toxicity, its inhibition presents a promising strategy for AD treatment. In this study, a series of new benzothiazolylurea analogues have been prepared and evaluated *in vitro* for their potency to inhibit ABAD/ 17β-HSD10 enzymatic activity. The most potent compounds have also been tested for their cytotoxic properties and their ability to permeate through blood-brain barrier has been predicted. To explain the structure-activity relationship QSAR and pharmacophore studies have been performed. *Results and Conclusions*: Compound **12** was identified being the most promising hit compound with good inhibitory activity (IC_{50} = 3.06 ± 0.40μM) and acceptable cytotoxicity profile comparable to the parent compound of frentizole.

The satisfactory physical-chemical properties suggesting its capability to permeate through BBB make compound 12 a novel lead structure for further development and biological assessment.

Keywords

Alzheimer's disease, amyloid-beta binding alcohol dehydrogenase (ABAD), 178-hydroxysteroid dehydrogenase type 10 (178-HSD10), chemical synthesis, enzyme inhibition, frentizole, QSAR, pharmacophore modelling

Graphical abstract

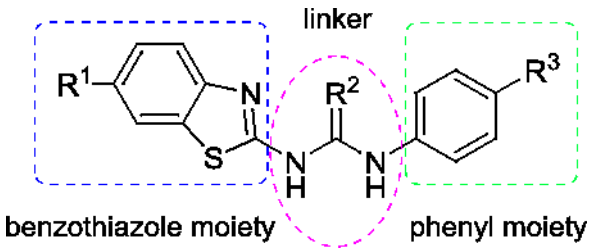

Introduction

Alzheimer's disease (AD) is the most common cause of senile dementia. About 20 million people worldwide suffer from this devastating illness [1]. AD is characterized by progressive decline of cognitive functions and memory. Despite intensive research, the pathogenic mechanisms of AD are still not fully understood and consequently no effective treatment has been yet developed.

The main pathological hallmarks of AD represents extracellular amyloid-beta peptide (Aβ) deposits also termed senile plaques, intracellular deposits of phosphorylated τ-protein, termed neurofibrillary tangles, and loss of neurons [2,3]. Although the aetiology of AD is still not known, buildup of Aβ is considered to play an important part in disease progression. The original amyloid cascade hypothesis suggested that extracellular plaques are the main toxic form of Aβ. However, recent data indicates that soluble intracellular oligomers are responsible for most of Aβ toxicity [4–8].

Inside the cell, Aβ interacts with a number of proteins including amyloid-binding alcohol dehydrogenase (ABAD), also referred as 17β-hydroxysteroid dehydrogenase type 10 (17β-HSD10) [9], an enzyme located within mitochondrial matrix capable to catalyse oxidation of alcohols and reduction of aldehydes and ketones.

As cells expressing catalytically inactive mutants of ABAD/ 17β-HSD10 show decreased sensitivity to Aβ, it has been suggested that the ABAD/ 17β-HSD10 enzymatic activity is required for mediating Aβ toxicity [10]. Therefore, inhibition of ABAD/ 17β-HSD10 is a possible strategy for AD treatment, which has already been indicated with the use of a small molecule ABAD/ 17β-HSD10 inhibitor AG18051. AG18051 is an irreversible ABAD/ 17β-HSD10 inhibitor reported to create a covalent bond with the cofactor NAD^+ within the enzyme's active site, and was shown subsequently to ameliorate Aβ toxicity in cell based studies [11,12].

Previously, frentizole and its analogues were found to be inhibitors of the ABAD-Aβ interaction, which presents another approach of targeting ABAD/ 17β-HSD10 for AD treatment [13,14]. Assuming that this effect was due to binding of these compounds to ABAD/ 17β-HSD10, some frentizole analogues were also tested as ABAD/ 17β-HSD10 inhibitors, which led to the discovery of a novel class of ABAD/ 17β-HSD10 inhibitors [15]. Similarly to AG18051, this new class of ABAD/ 17β-HSD10 inhibitors have cytoprotective effects in cells treated with Aβ [12,15].

Additionally to AD treatment ABAD/ 17β-HSD10 inhibition could be also employed in treatment of certain types of prostatic cancer, where overexpression of ABAD/ 17β-HSD10 takes place allowing the cancer cells to generate 5α-dihydrotestosterone in the absence of testosterone [16,17].

However, currently known ABAD/ 17β-HSD10 inhibitors (Fig. 1) suffer from some considerable drawbacks making them poor lead drug-like candidates. Compound AG18051 creates a covalent bond with NAD^+ cofactor within the enzyme's active site and with such mechanism of action it is likely to affect also other NAD+ dependant enzymes [11]. Compound RM-532-46 could suffer from specificity

issues as well, because it comprises a steroidal structural scaffold, which could be recognized by other steroid-binding sites [18]. Recently identified phosphonate-benzothiazole inhibitors showed rather poor activity with best compound having IC_{50} value of 52.7 μM [15]. Hence there is a need for developing novel ABAD/ 17β-HSD10 inhibitors with improved properties.

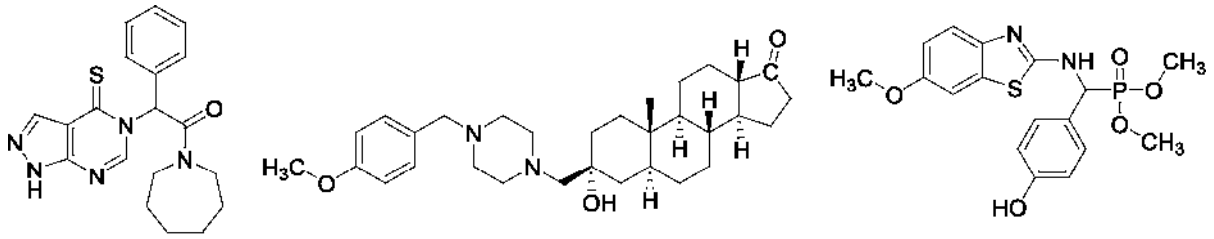

Figure 1: Currently known ABAD/ 17β-HSD10 inhibitors and their IC_{50} values.

In this study we have designed, synthesized and evaluated in vitro a series of novel 6-benzothiazolyl ureas, thioureas and guanidines. The most promising compounds have been further assessed for their cytotoxic properties and ability to cross the blood-brain barrier (BBB).

2. MATERIALS AND METHODS

2.1 General chemistry

Solvents and reagents were purchased from Fluka and Sigma-Aldrich (Czech Republic) and used without further purification. Reactions were monitored by TLC performed on aluminium sheets precoated with silica gel 60 F_{254} (Merck, Czech Republic) using mobile phase $CHCl_3$/MeOH 50:1 – 5:1 and detected under 254 nm UV light. Column chromatography was performed on silica gel 60 (230 mesh). Melting points were measured on Stuart SMP30 melting point apparatus (Bibby Scientific Limited, Staffordshire, UK) and are uncorrected.

NMR spectra were recorded at Varian Gemini 300 (^{1}H 300 MHz, ^{13}C 75 MHz, Palo Alto CA, USA) or Varian S500 (^{1}H 500 MHz, ^{13}C 126 MHz, Palo Alto CA, USA). In all cases, the chemical shift values for ^{1}H spectra are reported in ppm (δ) relative to residual $CHD_2SO_2CD_3$(δ 2.50), shift values for ^{13}C spectra are reported in ppm (δ) relative to solvent peak dimethylsulfoxide-d_6 (δ 39.52) [19].

Mass spectra (MS, respectively, MSn) were recorded on a LTQ XL linear ion trap mass spectrometer and evaluated using Xcalibur v 2.5.0 software (both Thermo Fisher Scientific, San Jose, CA, USA). The sample was dissolved in methanol (HPLC grade; Sigma-Aldrich, Prague, Czech Republic) and injected continuously (10 μL/min) by using a Hamilton syringe into the electrospray ion source. The parameters of electrospray were set up as follows: sheath gas flow rate 20 arbitrary units, aux gas

flow rate 10 arbitrary units, sweep gas flow rate 0 arbitrary units, spray voltage 4.5 kV, capillary temperature 275 °C, capillary voltage 13 V, tube lens 100 V.

For HRMS determination, a Dionex UltiMate 3000 analytical LC-MS system coupled with a Q Exactive Plus hybrid quadrupole-orbitrap spectrometer (both produced by ThermoFisher Scientific, Bremen, Germany) was used. The LC-MS system consisted of a binary pump HPG-3400RS connected to a vacuum degasser, a heated column compartment TCC-3000, an autosampler WTS-3000 equipped with a 25 µL loop and a VWD-3000 ultraviolet detector. A Waters Atlantis dC18 100Å (2.1 x 100mm/3µm) column was used as the stationary phase. The analytical column was protected against mechanical particles by an in-line filter (Vici Jour) with a frit of 0.5µm pores. Water (MFA) and acetonitrile (MFB) used in the analyses were acidified with 0.1% (v/v) of formic acid. Ions for mass spectrometry (MS) were generated by heated electro-spray ionization source (HESI) working in positive mode, with the following settings: sheath gas flow rate 40, aux gas flow rate 10, sweep gas flow rate 2, spray voltage 3.2 kV, capillary temperature 350°C, aux gas temperature 300°C, S-lens RF level 50, microscans 1, maximal injection time 35ms, resolution 140 000. The full-scan MS analyses monitored ions within m/z range 100 – 1500. The studied compounds were dissolved in methanol and 1µL of the solution was injected into the LC-MS system. For elution, following ramp-gradient program was used: 0 – 1 min: 10% MFB, 1 – 4 min: 10% – 100% MFB, 4 – 5 min: 100% MFB, 5 – 7.5 min: 10% MFB. The flow-rate in the gradient elution was set to 0.4 mL/min. To increase the accuracy of HRMS, internal lock-mass calibration was employed using polysiloxane traces of m/z = 445.12003 ($[M+H]^+$, $[C_2H_6SiO]_6$) present in the mobile phases. The chromatograms and mass spectra were processed in Chromeleon 6.80 and Xcalibur 3.0.63 software, respectively.

Elemental analysis (EA) was measured at Perkin-Elmer CHN Analyser 2400 Series II apparatus.

2.2 Physical-chemical properties calculation and measurement

Physical-chemical properties of prepared compounds in the unionized form were calculated in ACDLabs PhysChem Suite 2014 [20].

The method of measurement and calculation of ElogP was adapted from Technical guide OECD No. 117 [21]. Based on this method, the ElogD was determined accordingly [22]. All chemicals were purchased from Sigma-Aldrich (St. Louis, MO, USA). Seven standard stock solutions were prepared by dissolving nitrobenzene (ReagentPlus, 99%), chlorobenzene (puriss. p.a., ACS reagent, ≥99.5%), thymol (≥99.0%), biphenyl (ReagentPlus, 99.5%), butylbenzene (≥99%), fluoranthene (98%) and 4,4’-DDT (98%) in HPLC grade methanol and stored in the refrigerator at temperature of 4 °C. Mixed standard solution was prepared prior analysis by adding each of the stock standard solutions (100 µL) to 1.5 mL glass vial and addition of HPLC grade methanol (300 µL). Standard solution for dead time measurement was prepared by dissolving of citric acid (1 mg) in 70% solution of HPLC grade methanol and 30%

distilled water (1 mL). The Tris-HCl buffer for mobile phase was prepared from 0.05 M tris(hydroxymethyl)aminomethane solution by adjusting by 1 M HCl to pH 7.4. The pH measurement was carried by multimeter inoLab Multi 9430 IDS (WTW, Weilheim, DEU) with attached electrode SenTix Mic (WTW, Weilheim, DEU), DuraCal pH buffers (Hamilton, Bonduz, CHE) were used for calibration of pH electrode. All used water was prepared by Ultrapore Simplicity Water Purification System type 1 (Merck Millipore, Billerica, MA, USA).

The synthesized sample (1 mg) was dissolved in solution of 70% HPLC grade methanol and 30% distilled water (1 mL). Sample solutions were centrifuged using an Eppendorf Centrifuge 5418 (Eppendorf, Hamburg, Germany) for 10 minutes in frequency of 14000 rounds per minute and 0.9 mL of centrifuged supernatants was transferred to 1.5 mL glass vials. The analysis was performed by HPLC system Infinity 1260 (Agilent Technologies, Santa Clara, CA, USA) with Infinity 1290 auto sampler (G4226A), Infinity 1260 Quaternary LC pump (G1311B), Infinity 1260 Thermostatted Column Compartment (G1316A), and Infinity 1260 Diode-Array Detector (G4212B). Used LC column was Kinetex® 5 µm C18 100 Å, 100 x 4.6 mm (Phenomenex, Torrance, CA, USA) with attached SecurityGuardTM system for C18 HPLC column (Phenomenex, Torrance, CA, USA). Duration of the analysis was set to 60 min in flow rate of mobile phases 1 mL/min and at a temperature of 20 °C within the column. Dosage of sample and standard solution from autosampler was set to 10 µL. There was isocratic flow of mobile phases with 70% HPLC grade methanol and 30% distilled water for ElogP measurement and 70% HPLC grade methanol and 30% 0.05 M Tris-HCl buffer (pH 7.4) for ElogD measurement respectively. Both, analyses of standard solution and sample solutions were performed in triplicate.

The capacity factors (Eq. 1) were calculated from retention times of samples or standards:

$$k = \frac{t_r - t_0}{t_0} \qquad \text{(Eq. 1)}$$

k = capacity factor; t_0 = dead time (retention time of citric acid); t_r = retention time of sample

The ElogP values were calculated (Eq. 2). Linear regression coefficients were obtained from linear regression of ElogP of standard solutions against the log of their capacity factors. The ElogD values were calculated from measurement with 0.05 M Tris-HCl buffer (pH 7.4) as mobile phase B, using same standard solutions and equations.

$$\text{Elog}P = a + b \times \log k \qquad \text{(Eq. 2)}$$

P = octanol/water partition coefficient; a, b = linear regression coefficients; k = capacity factor

2.3 ABAD/ 17β-HSD10 Purification and Initial Compound Screens

Recombinant ABAD/ 17β-HSD10 was purified from *E.coli* as described in Aitken *et al.* 2016 [23]. Hroch *et al.* 2016 [24] was used as a reference to assess the capability of the synthesised benzothiazole urea analogues to modulate ABAD/ 17β-HSD10 activity, two initial compound screens were performed. Reaction conditions consisted of ABAD enzyme (0.5 µg/mL, 18.52 nM), NADH (250 µM), acetoacetyl-CoA (120 µM) and a single compound of interest (25 µM or 100 µM) (1% DMSO (v/v)). Solutions were prepared in assay buffer (10 mM HEPES buffer, pH 7.4 at 37 °C). Control solutions containing an equivalent concentration of DMSO (1% (v/v)) were also prepared and run concurrently. Reaction progression was measured via a decrease in NADH absorbance at 340 nm using a SpectraMAX M2e spectrophotometer. A reaction time of 200 s was employed yielding steady state conditions ($R^2 > 0.9$).

A test for compound active site cysteine residue binding was performed by comparing the inhibition observed with compounds **5** and **12** using the conditions described for the initial compound screen, in the presence and absence of DTT (5 mM).

Dose Response Relative IC50 values were measured using the reaction conditions outlined for the initial compound screen, the inhibitory nature of promising compounds was assessed over a range of concentrations (250 µM to 10 nM). Statistical analysis was performed with using GraphPad Prism.

To validate in-house ABAD assay, an IC50 curve was generated for compound AG18051 (the Kissinger inhibitor), a known potent inhibitor of the ABAD enzyme. An IC_{50} value of 69 nM was generated for compound AG18051 (Fig. 2), comparable to the 92 nM reported previously by Kissinger *et al*., using a cell based system [25], thus providing evidence that our screening assay is robust in nature.

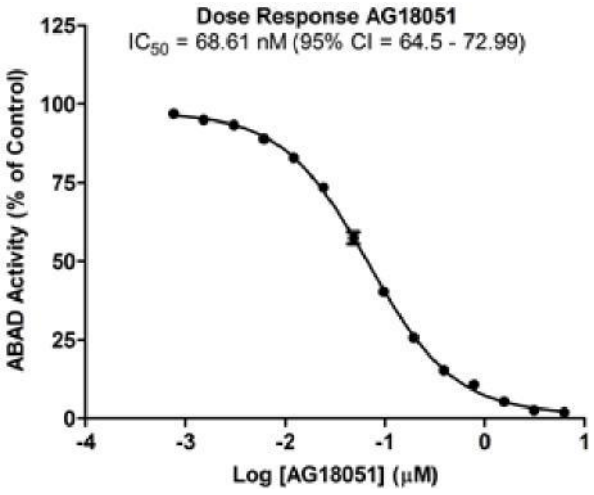

Figure 2: Dose response for compound AG18051. Values shown are an average ± SEM taken from two experiments each with three technical repeats.

2.4 QSAR analyses and Pharmacophore modelling

The relationship between the structures of the studied compound **1-15** and their inhibition potency towards ABAD/178-HSD10 was analysed by a systematic QSAR analysis. All compounds were prepared for QSAR analyses in HyperChem 8.0 [26] by running a 10 ps long molecular dynamic simulation at constant temperature 310.15K (step 1 fs, bath relaxation time 0.1 ps) using a semi-empirical method PM3. After the molecular dynamic simulation phase, the structures were geometrically optimized by Polak-Ribiére conjugate algorithm employing the same PM3 method with the convergence criterion set to 0.03 kcal/(Å.mol). The optimized structures along with the calculated Mulliken charges were imported into Dragon 6 program to generate 4885 various molecular descriptors (e.g. constitutional indices, topological indices, information indices, 2D matrix based descriptors, geometrical descriptors, 3D-MoRSE descriptors, WHIM descriptors, GETAWAY descriptors, drug-like properties, etc.) [27]. The matrix of molecular descriptors and the relative ABAD/17β-HSD10 inhibitions caused by 25 mM were processed in a self-developed C++ based program Statoo using multiple linear regression (MLR) and an exhaustive combinatorial variable selection algorithm evaluating every *k*-set of molecular descriptors [28]. With the respect to recommended ratio of 1 predictor to 5 or more compounds, we investigated all possible MLR QSAR models containing at most 3 molecular descriptors [29]. The final MLR QSAR top-scoring model was evaluated by leave-one-out, leave-30%-out cross-validation, and also by randomization and scrambling the vector of biological activities [30]. The domain of applicability of the best MLR QSAR model was checked by Williams plot in Matlab 2015.

In order to reveal the most significant structural features of the studied compound for the observed biological activity (i.e. at concentration 25 mM), a pharmacophore analysis was performed. Initially, the models of **1-15** were prepared by quenched molecular dynamics (QMD) in Open3DAlign program [31], which uses Tinker to perform molecular mechanics calculations with MMFF94 force field. The QMD protocol was set to carry out a 10 ps simulation at 1000K in vacuum (step size 0.1 fs) and to minimize the geometry till the gradient achieved 0.001 kcal/(Å.mol) or the number of iterations exceeded 1000. For each compound in the set, a conformer library was prepared to be screened in 3D alignment process. A hybrid approach mixing Pharao pharmacophore-based [32] and LAMBDA-like [33] algorithms in Open3DAlign program was utilized to find the best superimposition of all the studied structures on compound **12**. Within the alignment process, all combinations between **12** conformers and the other compounds' conformers were aligned to find a superimposition exhibiting maximal O3A score [34]. The best molecular superimposition in the sense of the highest O3A score was investigated by a pharmacophore analysis in LigandScout 3.1 program to derive the substructure influencing most significantly the biological activity. The pharmacophore hypothesis was derived using the most active compounds as a training set.

2.5 Cell viability assessment

The effect of compounds on the cell viability was examined using methodology combining LDH and MTT assay into one experimental setup. Such an assay has been chosen due to the fact that widely used MTT test is partially dependent on the mitochondrial oxidoreductases [35], whose activity might be influenced by the tested compounds targeted to mitochondria. The protocol for this assay has been described previously [36]. Briefly CHO cell line (Chinese hamster ovary, CHO-K1WT2, CRL-1984 ECACC, Salisbury, UK) were cultured according to ECACC recommended conditions and seeded in a density of 8 000 cells per well as was described earlier [37]. Tested compounds were dissolved in DMSO and subsequently in the growth medium (F-12) supplemented with 1% PEN/STREP without FBS so that the final concentration of DMSO did not exceed 0.5% (v/v). Cells were exposed to a tested compound in the medium (100 µL) for 24 hours. Then 10 µL of MTT (2.5 mg/mL in buffer) was added and 50 µL of the culture supernatant was transferred to a new plate yet containing 50 µL of LDH substrate mixture consisting of lactate (2.5 mg/mL), NAD (2.5 mg/mL), phenazine methansulphate (100 µM) and Triton X-100 (0.1%) in Tris–HCl buffer (pH 8.2). LDH reaction mixture was incubated at 37 °C for 15-30 min until the difference between negative (no treatment) and positive control (0.1% Triton X-100) was obvious. Cellular fraction containing MTT was allowed to produce formazan for another approximately 3 h at 37°C. Thereafter, medium with MTT was removed and crystals of formazan were dissolved in DMSO (100 µL). Absorbance was measured at 570 nm with 650 nm reference wavelength on Synergy HT reader (BioTek, USA) for both LDH and MTT fraction. IC_{50} was then calculated from the control - subtracted triplicates using non-linear regression (four parameters) of GraphPad Prism 5 software. Final IC_{50} and SEM value was obtained as a mean of at least 3 independent measurements (in triplicate).

3. EXPERIMENTAL

3.1 Chemical preparation

2-aminobenzo[d]thiazole-6-carboxylate

Ethyl 4-aminobenzoate (1 eq.) and KSCN (4 eq.) were dissolved in acetic acid (4 mL/mmol) and stirred at rt for 20 mins. Then the reaction mixture was cooled to 10 °C and bromine (2 eq.) dissolved in small amount of acetic acid was added dropwise. Afterwards the reaction mixture was left to warm up to rt and stirred overnight. After the reaction was completed (monitored by TLC), reaction mixture was added dropwise into the sat. aq. NH_3 solution (15 mL/mmol) while cooling in an ice bath. The product was extracted to EtOAc and the organic layer was washed with $Na_2S_2O_3$, sat. aq. $NaHCO_3$ and brine, dried using anhydrous Na_2SO_4 and concentrated under reduced pressure. The crude product was either recrystallized from diethylether to obtain ethyl 2-aminobenzo[*d*]thiazole-6-carboxylate in 69% yield.

^{1}H NMR (500 MHz, DMSO-d_6): δ (ppm) 8.27 (d, *J* = 1.8 Hz, 1H), 7.88 (s, 2H), 7.81 (dd, *J* = 8.4, 1.8 Hz, 1H), 7.36 (d, *J* = 8.4 Hz, 1H), 4.27 (q, *J* = 7.1 Hz, 2H), 1.30 (t, *J* = 7.1 Hz, 3H).

General procedure for synthesis of N-(benzo[d]thiazol-2-yl)-1H-imidazole-1-carboxamides

Corresponding 2-aminobenzo[*d*]thiazole (1 eq.) was dissolved in a mixture of dimethylformamide (DMF) and dichloromethane (DCM) (1:6; 12 mL/mmol), 1,1'-carbonyldiimidazole (CDI; 1.2 eq.) was added and the reaction mixture was stirred vigorously at reflux overnight. The resulting precipitate was collected by filtration, washed with DCM and dried to obtain corresponding *N*-(benzo[*d*]thiazol-2-yl)-1*H*-imidazole-1-carboxamide as a white solid in excellent yield (90 - 97 %).

General procedure for synthesis of N-(benzo[d]thiazol-2-yl)-1H-imidazole-1-carbothioamides

Corresponding 2-aminobenzo[*d*]thiazole (1 eq.) was dissolved in acetonitrile (MeCN; 5 mL/mmol), 1,1'-thiocarbonyldiimidazole (SCDI; 1.2 eq.) was added and the reaction mixture was stirred at reflux overnight. The resulting precipitate was collected by filtration, washed with DCM and dried to obtain corresponding *N*-(benzo[*d*]thiazol-2-yl)-1*H*-imidazole-1-carbothioamide as a pale yellow solid in medium to excellent yield (65 - 95 %).

General procedure for synthesis of 1-(benzo[d]thiazol-2-yl)-3-phenylureas resp. 1-(benzo[d]thiazol-2-yl)-3-phenylthioureas

Corresponding *N*-(benzo[*d*]thiazol-2-yl)-1*H*-imidazole-1-carboxamide resp. *N*-(benzo[*d*]thiazol-2-yl)-1*H*-imidazole-1-carbothioamide (1 eq.) was dissolved in DMF (8 mL/mmol), the corresponding aniline derivative (1.1 eq.) was added and the reaction mixture was stirred at 60 °C. After the reaction was completed (monitored by TLC), the reaction mixture was portioned with 1 M HCl aqueous solution (for carboxyl group containing aniline derivatives). The resulting precipitate was collected by filtration, washed with water and dried to obtain corresponding 1-(benzo[*d*]thiazol-2-yl)-3-phenylurea or 1-(benzo[*d*]thiazol-2-yl)-3-phenylthiourea in medium to excellent yield (60 - 96 %).

General procedure for synthesis of 1-(benzo[d]thiazol-2-yl)-3-phenylguanidines

The corresponding thiourea derivative (1 eq.) was dissolved in 7N methanolic ammonia solution (12 mL/mmol), mercury oxide (3 eq.) was added and the reaction mixture was stirred at room temperature overnight. After the reaction was completed (monitored by TLC), the reaction mixture was filtered over Celite and washed with either THF or MeOH (40 mL/mmol). Evaporation of the filtrate gave corresponding guanidine in poor to good yield (10–79 %). In cases, where further purification was required, the procedure is described together with the respective compound's characterization.

*Preparation of hydrochloride salt from guanidine base **12***

The guanidine **12** was dissolved in THF, purged with diethylether saturated with gaseous hydrochloric acid and stirred for 1 h at 0 °C. The resulting precipitate was collected by filtration and washed with diethyl ether to obtain guanidine hydrochloride as white solid (90%).

3.2 Prepared compounds and their characterization

1-(6-methoxybenzo[*d*]thiazol-2-yl)-3-phenylurea (**1**, frentizole)

M.p. 328–330 °C. Yield 91%. ^{1}H NMR (500 MHz, DMSO-d_6): δ (ppm) 10.68 (br s, 1H), 9.13 (br s, 1H), 7.56 (d, *J* = 8.8 Hz, 1H), 7.54 – 7.47 (m, 3H), 7.33 (t, *J* = 7.9 Hz, 2H), 7.05 (t, *J* = 7.3 Hz, 1H), 6.98 (dd, *J* = 8.8, 2.6 Hz, 1H), 3.79 (s, 3H). ^{13}C NMR (126 MHz, DMSO-d_6): δ (ppm) 157.68, 155.87, 152.01, 142.82, 138.66, 132.61, 129.10, 123.08, 120.29, 118.95, 114.55, 105.12, 55.78. ESI-HRMS: *m/z*300.07986 $[M+H]^+$ (calc. for $C_{15}H_{13}N_3O_2S$: 300.08012$[M+H]^+$).

1-(6-methoxybenzo[*d*]thiazol-2-yl)-3-phenylthiourea (**2**)

M.p. 198–200 °C. Yield 88%. ^{1}H NMR (500 MHz, DMSO-d_6): δ (ppm) 12.51 (br s, 1H), 10.80 (br s, 1H), 7.70 (d, *J* = 7.9 Hz, 2H), 7.49 (m, 2H), 7.35 (t, *J* = 7.4 Hz, 2H), 7.14 (s, 1H), 7.02 (dd, *J* = 8.8, 2.3 Hz, 1H), 3.79 (s, 3H); ^{13}C NMR (126 MHz, DMSO-d_6): δ (ppm) 181.42, 156.09, 139.38, 128.44, 124.17, 122.87, 114.74, 105.93, 55.68; ESI-HRMS: *m/z*316.05685 $[M+H]^+$ (calc. for $C_{15}H_{13}N_3OS_2$: 316.05728$[M+H]^+$).

1-(6-methoxybenzo[*d*]thiazol-2-yl)-3-phenylguanidine (**3**)

The crude product was recrystallized from petroleum ether.

M.p. 129.5–131 °C. Yield79 %. ^{1}H NMR (500 MHz, DMSO-d_6): δ (ppm) 9.04 (br s, 1H), 7.96 (br s, 2H), 7.48 (dd, *J* = 8.5, 0.9 Hz, 2H), 7.46 (d, *J* = 8.8 Hz, 1H), 7.37 (d, *J* = 2.6 Hz, 1H), 7.35 – 7.30 (m, 2H), 7.08 – 7.01 (m, 1H), 6.90 (dd, *J* = 8.8, 2.7 Hz, 1H), 3.77 (s, 3H). ^{13}C NMR (126 MHz, DMSO-d_6): δ (ppm) 171.47, 155.27, 153.69, 145.64, 138.93, 131.80, 128.82, 122.83, 120.68, 119.53, 113.54, 104.94, 55.52. ESI-HRMS: *m/z* 299.09564 $[M+H]^+$ (calc. for $C_{15}H_{14}N_4OS$: 299.09611$[M+H]^+$).

1-(6-fluorobenzo[*d*]thiazol-2-yl)-3-phenylurea (**4**)

M.p. 362.5–364.4 °C. Yield 76%. ^{1}H NMR (500 MHz, DMSO-d_6): δ (ppm) 10.77 (br s, 1H), 9.06 (br s, 1H), 7.79 (dd, *J* = 8.7, 2.6 Hz, 1H), 7.71 – 7.61 (m, 1H), 7.51 (d, *J* = 7.8 Hz, 2H), 7.34 (t, *J* = 7.9 Hz, 2H), 7.21 (td, *J* = 9.2, 2.7 Hz, 1H), 7.07 (t, *J* = 7.4 Hz, 1H). ^{13}C NMR (126 MHz, DMSO-d_6): δ (ppm) 159.20, 158.14 (d, *J* = 239.3 Hz), 151.64, 144.93, 138.10, 132.39, 128.63 (d, *J* = 15.5 Hz), 122.84 (d, *J* = 8.3 Hz), 120.28, 118.79 (d, *J* = 16.6 Hz), 113.48 (dd, *J* = 24.3, 14.2 Hz), 107.70 (dd, *J* = 26.9, 13.5 Hz). ESI-HRMS: *m/z*288.05988 $[M+H]^+$ (calc. for $C_{14}H_{10}FN_3OS$: 288.06014$[M+H]^+$).

1-(6-fluorobenzo[*d*]thiazol-2-yl)-3-phenylthiourea (**5**)

M.p. 302 °C decomp. Yield 84%. ^{1}H NMR (300 MHz, DMSO-d_6): δ (ppm) 12.52 (br s, 1H), 10.81 (br s, 1H), 7.81 (dd, *J* = 9.0, 2.1 Hz, 1H), 7.69 (d, *J* = 8.4 Hz, 2H), 7.55 (s, 1H), 7.36 (t, *J* = 7.9 Hz, 2H), 7.27 (td, *J* = 9.2, 2.5 Hz, 1H), 7.21 – 7.06 (m, 1H); ^{13}C NMR (75 MHz, DMSO-d_6): δ (ppm) 180.89, 158.50 (d, *J* = 239.2 Hz), 157.48, 139.25, 128.48, 124.52, 123.21, 114.37 (d, *J* = 24.6 Hz), 108.97 (d, *J* = 27.2 Hz); ESI-HRMS: *m/z*304.03711 $[M+H]^+$ (calc. for $C_{14}H_{10}FN_3S_2$: 304.03729$[M+H]^+$).

1-(6-fluorobenzo[*d*]thiazol-2-yl)-3-phenylguanidine (**6**)

The crude product was recrystallized from petroleum ether/heptan.

M.p. 166–168 °C. Yield 32%. ^{1}H NMR (500 MHz, CD_3OD): δ (ppm) 7.51 (dd, *J* = 8.8, 4.8 Hz, 1H), 7.44 – 7.33 (m, 5H), 7.15 (tt, *J* = 7.4, 1.3 Hz, 1H), 7.03 (td, *J* = 9.1, 2.7 Hz, 1H). ^{13}C NMR (126 MHz, CD_3OD): δ (ppm) 174.60, 160.27 (d, *J* = 239.6 Hz), 156.54, 149.69, 139.25, 133.70 (d, *J* = 10.7 Hz), 130.28, 125.78, 123.96, 121.04 (d, *J* = 8.9 Hz), 114.00 (d, *J* = 24.3 Hz), 108.14 (d, *J* = 27.0 Hz). ESI-HRMS: *m/z*287.07584 $[M+H]^+$ (calc. for $C_{14}H_{11}FN_4S$: 287.07612$[M+H]^+$).

ethyl 2-(3-phenylureido)benzo[*d*]thiazole-6-carboxylate (**7**)

M.p. 314–316 °C. Yield 59%. ^{1}H NMR (500 MHz, DMSO-d_6): δ (ppm) 11.12 (br s, 1H), 9.23 (br s, 1H), 8.56 (d, *J* = 0.8 Hz, 1H), 7.97 (dd, *J* = 8.5, 1.8 Hz, 1H), 7.72 (d, *J* = 8.4 Hz, 1H), 7.53 (d, *J* = 7.7 Hz, 2H), 7.34 (t, *J* = 7.9 Hz, 2H), 7.07 (t, *J* = 7.4 Hz, 1H), 4.33 (q, *J* = 7.1 Hz, 2H), 1.34 (t, *J* = 7.1 Hz, 3H). ^{13}C NMR (126 MHz, DMSO-d_6): δ (ppm) 165.49, 162.76, 151.89, 138.25, 131.45, 128.93, 127.06, 124.17, 123.41, 123.13, 119.08, 118.88, 60.64, 14.23. ESI-HRMS: *m/z* 342.09009 $[M+H]^+$ (calc. for $C_{17}H_{15}N_3O_3S$: 342.09069$[M+H]^+$)

ethyl 2-(3-phenylthioureido)benzo[*d*]thiazole-6-carboxylate (**8**)

M.p. 207.5–208.8 °C. Yield 88%. ^{1}H NMR (500 MHz, DMSO-d_6): δ (ppm) 10.61 (s, 1H), 8.48 (s, 1H), 7.99 (dd, *J* = 8.4, 1.6 Hz, 1H), 7.69 (d, *J* = 7.9 Hz, 2H), 7.60 (s, 1H), 7.37 (t, *J* = 6.9 Hz, 2H), 7.16 (s, 1H), 4.33 (q, *J* = 7.1 Hz, 2H), 1.33 (t, *J* = 7.1 Hz, 3H). ^{13}C NMR (126 MHz, DMSO-d_6): δ (ppm) 181.89, 165.35, 156.99, 139.18, 128.55, 128.48, 127.74, 124.73, 124.01, 123.41, 112.48, 60.79, 14.27. ESI-HRMS: *m/z*358.06760 $[M+H]^+$ (calc. for $C_{17}H_{15}N_3O_2S_2$: 358.06784$[M+H]^+$).

ethyl 2-(3-phenylguanidino)benzo[*d*]thiazole-6-carboxylate (**9**)

The crude product was recrystallized from petroleum ether/heptan.

M.p. 134–136 °C. Yield 28%. ^{1}H NMR (500 MHz, DMSO-d_6): δ (ppm) 9.31 (br s, 1H), 8.36 (s, 1H), 8.14 (br s, 1H), 7.89 (d, *J* = 8.2 Hz, 1H), 7.59 (d, *J* = 8.4 Hz, 1H), 7.46 (d, *J* = 7.1 Hz, 2H), 7.36 (t, *J* = 7.7 Hz, 2H), 7.10 (t, *J* = 7.1 Hz, 1H), 4.31 (dd, *J* = 14.0, 6.9 Hz, 2H), 1.33 (t, *J* = 7.1 Hz, 3H). ^{13}C NMR (126 MHz, DMSO-

d_6): 6 (ppm) 176.24, 165.56, 155.35, 154.57, 138.31, 130.74, 128.93, 126.78, 123.54, 122.58, 121.43, 118.38, 60.49, 14.23. ESI-HRMS: m/z341.10617 $[M+H]^+$ (calc. for $C_{17}H_{16}N_4O_2S$: 341.10667$[M+H]^+$).

1-(6-methoxybenzo[d]thiazol-2-yl)-3-(4-methoxyphenyl)urea (**10**)
M.p. 316–318 °C. Yield 87%. ^{1}H NMR (500 MHz, DMSO-d_6): 6 (ppm) 10.59 (br s, 1H), 8.94 (br s, 1H), 7.55 (d, J = 8.7 Hz, 1H), 7.50 (d, J = 2.3 Hz, 1H), 7.41 (d, J = 8.7 Hz, 2H), 6.98 (dd, J = 8.7, 2.2 Hz, 1H), 6.91 (d, J = 8.8 Hz, 2H), 3.79 (s, 3H), 3.73 (s, 3H). ^{13}C NMR (126 MHz, DMSO-d_6): 6 (ppm) 157.57, 155.64, 155.20, 151.87, 142.77, 132.48, 131.38, 120.70, 120.16, 114.30, 114.09, 104.92, 55.59, 55.20. ESI-HRMS: m/z330.09015 $[M+H]^+$ (calc. for $C_{16}H_{15}N_3O_3S$: 330.09069$[M+H]^+$).

1-(6-methoxybenzo[d]thiazol-2-yl)-3-(4-methoxyphenyl)thiourea (**11**)
M.p. 202.2–202.7 °C. Yield 90%. ^{1}H NMR (500 MHz, DMSO-d_6): 6 12.33 (br s, 1H), 11.04 (br s, 1H), 7.60 – 7.40 (m, 4H), 7.01 (dd, J = 8.8, 2.6 Hz, 1H), 6.93 (d, J = 8.8 Hz, 2H), 3.79 (s, 3H), 3.76 (s, 3H). ^{13}C NMR (126 MHz, DMSO-d_6): 6 (ppm) 179.76, 160.68, 156.49, 156.06, 138.31, 132.03, 129.52, 125.22, 118.05, 114.61, 113.63, 105.76, 55.66, 55.24. ESI-HRMS: m/z346.06763 $[M+H]^+$ (calc. for $C_{16}H_{15}N_3O_2S_2$: 346.06784$[M+H]^+$).

1-(6-methoxybenzo[d]thiazol-2-yl)-3-(4-methoxyphenyl)guanidine (**12**)
M.p. 160.5–161.7 °C. Yield 72%. ^{1}H NMR (500 MHz, DMSO-d_6): 6 (ppm) 8.96 (br s, 1H), 7.82 (s, 1H), 7.43 (d, J = 8.8 Hz, 1H), 7.37 – 7.29 (m, 3H), 6.96 – 6.91 (m, 2H), 6.89 (dd, J = 8.8, 2.6 Hz, 1H), 3.76 (s, 3H), 3.74 (s, 3H). ^{13}C NMR (126 MHz, DMSO-d_6): 6 (ppm) 171.74, 155.71, 155.14, 154.33, 145.77, 131.66, 131.35, 123.57, 119.28, 114.15, 113.37, 104.97, 55.51, 55.22. ESI-HRMS: m/z329.10632 $[M+H]^+$ (calc. for $C_{16}H_{16}N_4O_2S$: 329.10667$[M+H]^+$).

4-(3-(6-methoxybenzo[d]thiazol-2-yl)ureido)benzoic acid (**13**)
M.p. 295 °C decomp. Yield 96%. ^{1}H NMR (500 MHz, DMSO-d_6): 6 (ppm) 10.52 (br s, 1H), 8.75 (br s, 1H), 7.94 – 7.89 (m, 2H), 7.67 – 7.61 (m, 2H), 7.57 (d, J = 8.8 Hz, 1H), 7.53 (d, J = 2.6 Hz, 1H), 7.00 (dd, J = 8.8, 2.6 Hz, 1H), 3.80 (s, 3H). ^{13}C NMR (126 MHz, DMSO-d_6): 6 (ppm) 166.96, 157.31, 155.83, 152.10, 142.98, 141.94, 132.38, 130.65, 124.57, 120.06, 117.58, 114.56, 104.99, 55.67. ESI-HRMS:m/z344.06989 $[M+H]^+$ (calc. for $C_{16}H_{13}N_3O_4S$: 344.06995$[M+H]^+$).

4-(3-(6-methoxybenzo[d]thiazol-2-yl)thioureido)benzoic acid (**14**)
M.p. 278 °C decomp. Yield 95%. ^{1}H NMR (500 MHz, DMSO-d_6): 6 (ppm) 12.67 (br s, 1H), 10.70 (br s, 1H), 7.91 (m, 4H), 7.49 (d, J = 2.4 Hz, 1H), 7.45 (d, J = 8.8 Hz, 1H), 7.04 (dd, J = 8.8, 2.5 Hz, 1H), 3.80 (s,3H).^{13}C NMR (126 MHz, DMSO-d6): d (ppm) 182.47, 167.17, 156.08, 143.81, 132.24, 129.89, 128.53,

125.15, 120.84, 115.32, 114.89, 106.10, 55.70. ESI-HRMS:m/z360.04681 $[M+H]^+$ (calc. for $C_{16}H_{13}N_3O_3S_2$: 360.04711$[M+H]^+$).

4-(3-(6-methoxybenzo[d]thiazol-2-yl)guanidino)benzoic acid (**15**)

The crude product was purified using column chromatography.

M.p. 275–277 °C. Yield 17%. ^{1}H NMR (500 MHz, DMSO-d_6): δ (ppm) 12.61 (br s, 1H), 9.38 (br s, 1H), 8.12 (br s, 2H), 7.91 – 7.87 (m, 2H), 7.63 (d, J = 8.5 Hz, 2H), 7.49 (d, J = 8.8 Hz, 1H), 7.40 (d, J = 2.6 Hz, 1H), 6.93 (dd, J = 8.8, 2.6 Hz, 1H), 3.78 (s, 3H). ^{13}C NMR (126 MHz, DMSO-d_6): δ (ppm) 171.03, 167.10, 155.47, 153.07, 145.49, 143.47, 132.04, 130.34, 124.30, 119.86, 118.95, 113.76, 104.94, 55.55. ESI-HRMS: m/z343.08539 $[M+H]^+$ (calc. for $C_{16}H_{14}N_4O_3S$: 343.08594$[M+H]^+$).

4. RESULTS AND DISCUSSION

Design of novel compounds originates from the previously identified ABAD/ 17β-HSD10 modulator frentizole and its analogues [13–15].Our novel compounds consist of three substructural parts i.e. a benzothiazole moiety [38], a linker and a phenyl moiety (Fig. 3). The benzothiazole moiety was substituted in position 6 with a methoxy group (the same as is found in the parent compound frentizole), fluorine or an ethylcarboxyl group were used at the same position to investigate whether a change in spatial size, lipophilicity or amount of hydrogen bond acceptors/donors (HBA/HBD) in this part of the molecule would result in a change of inhibitory ability. Three different linkers where used to investigate difference(s) between a hydrophilic urea (H-bond acceptor; present in parent compound frentizole), guanidine (H-bond donor) linkers and the rather more lipophilic thiourea linker. The phenyl moiety was either non-substituted (similar to the parent compound frentizole) or substituted in the 4-position with either a hydrophilic carboxyl and hydroxyl functional groups (capable of creating hydrogen bonds) or a slightly lipophilic methoxy moiety. Frentizole was also synthesized as a reference compound.

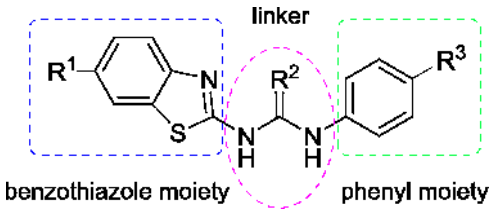

Figure 3: Design of novel frentizole analogues.

Generally, the synthesis started with activation of the corresponding 2-aminobenzo[*d*]thiazole using 1,1'-carbonyldiimidazole resp. 1,1'-thiocarbonyldiimidazole (Scheme 1),only the ethyl

2-aminobenzo[*d*]thiazole-6-carboxylate was prepared in a separate step by treating 4-aminobenzoatewith potassium thiocyanate and bromine in acetic acid (Scheme 1) [39].In the next step, the reactive imidazolyl intermediate was treated with the corresponding aniline to obtain a non-symmetrically substituted urea or thiourea product (Scheme 1).

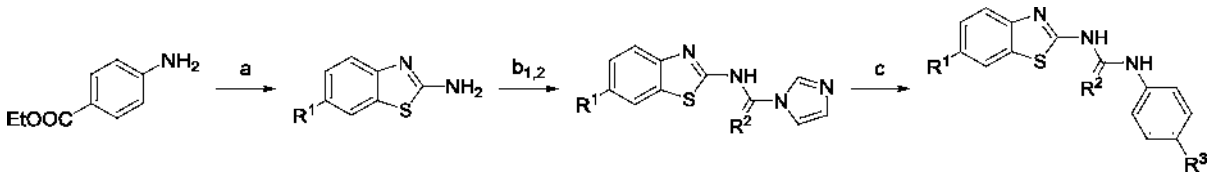

Scheme 1: Synthesis of urea and thiourea derivatives. Reagents and conditions:(a) KSCN, Br_2, AcOH, rt; (b_1) CDI,DCM/DMF, reflux; (b_2) SCDI, MeCN, reflux; (c) aromatic amine, DMF, 60°C.

Guanidine analogues were prepared by treating corresponding thiourea with mercury oxide in methanolic ammonia solution (Scheme 2). Guanidine hydrochloride with improved solubility in water (suitable for potential *in vivo* testing) was prepared by stirring guanidine base **12** in mixture of diethyl ether and THF saturated by gaseous hydrochloric acid (Scheme 2).

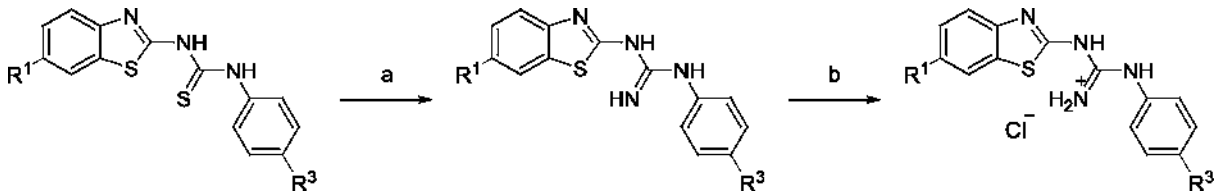

Scheme 2: Synthesis of guanidine analogues. Reagents and conditions: (a) NH_3, HgO, MeOH, rt; (b) sat. HCl in THF, Et_2O, rt.

The ability of the synthesised compounds to modulate ABAD/17β-HSD10 activity was assessed by a spectrophotometric assay that was formerly outlined by Hroch *et al.* [24]. An initial compound screen was performed using each compound at 100 μM concentration. All tested compounds, except of the standard frentizole, were found to be capable to markedly decrease the activity of the ABAD enzyme, with nine compounds (**2**, **4**, **5**, **8**, **9**, **11**–**14**) decreasing the activity by more than 50%.A subsequent compound screen was performed at 25 μM in an attempt to isolate the most potent inhibitors. At this lower concentration, compounds **2**, **5**, **9** and **12** were found to retain a similar level of inhibition as that seen at 100 μM, whilst the remaining inhibitors showed less marked inhibition (Table 1). Establishing of the SAR for the presented set of compounds was, however, a difficult task, as there were no clear correlations between the structure of compounds and their inhibitory activity.

There was only one observed trend when the thiourea linked compounds (e.g. **2** and **5**) showed mostly higher potency compared to the analogous ureas and guanidines. Nevertheless, the best inhibition was found for the guanidine **12**. Different substitutions of the benzothiazole and/or phenyl moieties of the parent frentizole had their effects on the compounds' activity, but without any obvious logical order.

Table 1: Relative ABAD/17β-HSD10 activity in the presence of each compound at concentrations of 100 µM and 25 µM (presented as % of control ± SEM). Values shown are an average of two independent experiments, each with three technical repeats.

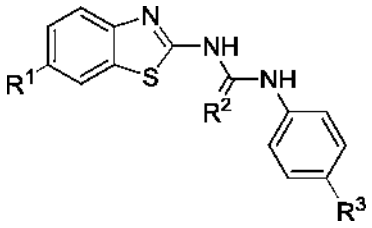

Compound	R1	R2	R3	100 µM (% Activity ± SEM)	25 µM (% Activity ± SEM)
control	---	---	---	100.0 ± 0.11	100.0 ± 0.20
frentizole (1)	OMe	O	H	102.9 ± 2.98	97.4 ± 0.82
2	OMe	S	H	34.8 ± 1.42	39.8 ± 0.44
3	OMe	NH	H	61.8 ±5.87	57.9 ±3.91
4	F	O	H	41.0 ± 0.61	69.2 ± 0.40
5	F	S	H	23.9 ± 0.69	29.0 ± 0.23
6	F	NH	H	81.0 ±4.78	86.6±1.43
7	COOEt	O	H	64.3 ±1.56	79.2 ±1.60
8	COOEt	S	H	36.6 ± 0.33	45.5 ± 0.33
9	COOEt	NH	H	35.6 ±2.45	32.0±3.00
10	OMe	O	OMe	62.2 ± 0.93	69.7 ± 0.42
11	OMe	S	OMe	46.9 ± 1.50	60.9 ± 0.74
12	OMe	NH	OMe	17.9 ± 0.71	17.0 ± 0.09
13	OMe	O	COOH	41.1 ± 0.47	62.4 ± 0.29
14	OMe	S	COOH	29.3 ± 0.76	47.0 ± 0.34
15	OMe	NH	COOH	86.0 ±6.23	104.2 ±4.32

To further assess the potency of the two most active inhibitors, compounds **5** and **12**, ABAD/17β-HSD10 activity was measured in the presence of increasing concentrations of the two inhibitors

and their IC_{50} values calculated using GraphPad Prism. Relative IC_{50} value of 3.06 ± 0.40 μM was found for compound **12** (Fig. 4).

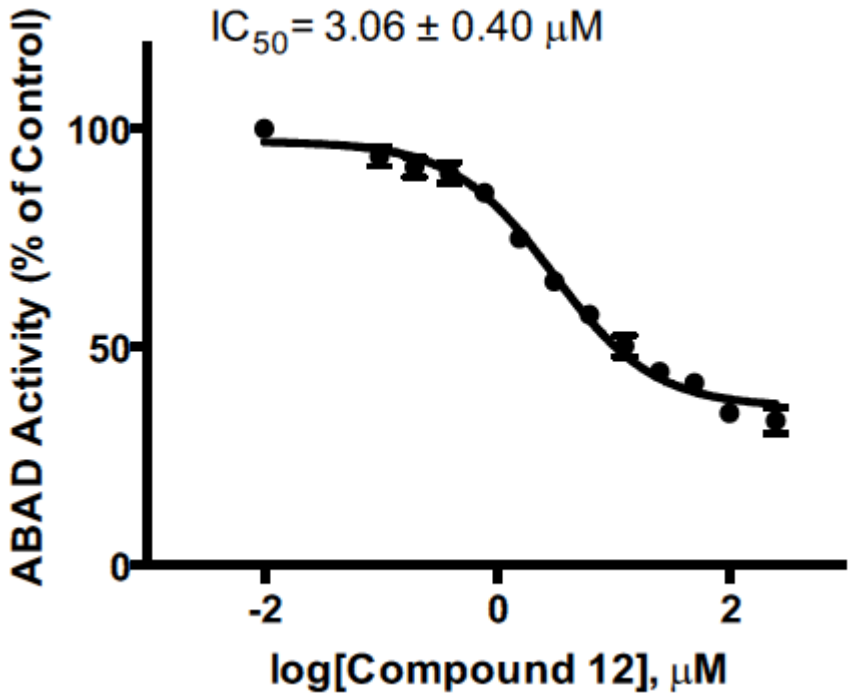

Figure 4: IC50 determination for compound **12.**

Compound 5 produced an inconclusive dose response curve and a relative IC_{50} value could not be determined. Further analysis of this compound revealed that the inhibition was reversed upon the addition of dithiothreitol (DTT), indicating the inhibition is likely due to the formation of a disulphide bond to an active site cysteine residue (Fig. 5). The DMSO control and 12 showed little change in ABAD/ 17β -HSD10 activity with inhibition remaining constant under the addition of DTT. However compound 5 showed a reversal in ABAD/ 17β -HSD10 inhibition upon the addition of DTT with activity values nearly returning to the control levels. As many other enzymes exhibit similar properties containing active site cysteine residues (e.g. tyrosine phosphatises [40]) this could prove difficult to obtain specificity for ABAD/178-HSD10 for such type of thiourea linked compounds. From this point of view, the thiourea moiety seems to be unlikely used for further design of ABAD/ 17β -HSD10 inhibitors for the lack of specificity.

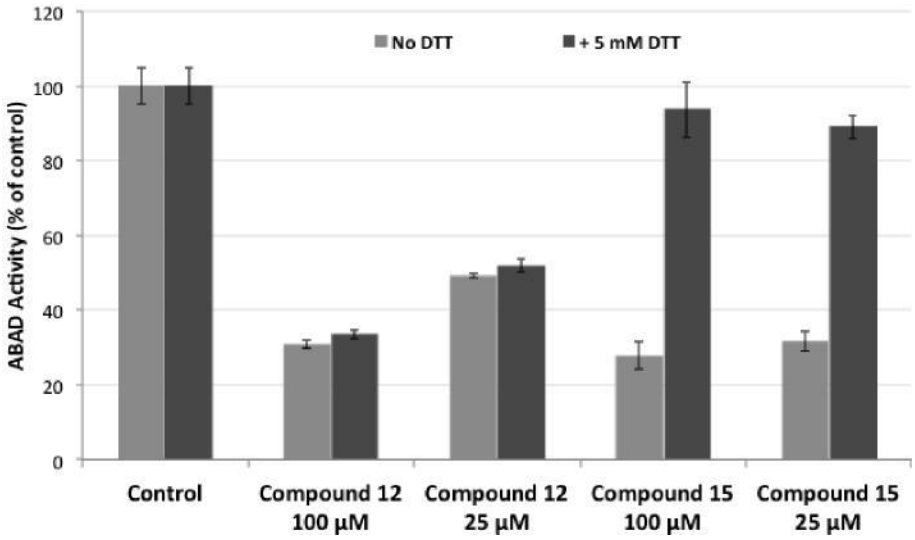

Figure 5: Relative ABAD/17β-HSD10 activity in the presence of each compound at concentrations of 25 µM and 100 µM with and without the addition of 5 mM DTT (presented as % of control ± SEM).

The cytotoxicity of the two most potent inhibitors **5** and **12** was assessed using LDH and MTT assay. Cytotoxicity assessment revealed that compound **12** is one order of magnitude less toxic when compared to 5 using two different assays and that its toxicity is at similar level and comparable to parent frentizole (Table 2). Both IC_{50} values obtained for **5** were found similar and it plausibly suggests that the compound 5does not affect the electron transport chain (ETC) of mitochondria (i.e. compound 5 does not inhibit enzymes of ETC) [35]. Differently in the case of compound **12**, the IC_{50} value obtained via a MTT assay was found lower than the LDH assay result, which could be hypothesized to its influence of ETC. However, only small differences between both assays were found that plausibly means only minor influence of mitochondrial ETC and should be further explored for this kind of molecules.

Table 2: Cytotoxicity assessment of frentizole and the most promising inhibitors **5** and **12.**

Compound	IC_{50} (µM ± SEM)	
	LDH	MTT
frentizole	46 ± 6	38 ± 5
5	3.5 ± 0.2	3.1± 0.4
12	51 ± 11	23± 6

The physical-chemical properties were calculated (ACDLabs PhysChem Suite 2014 [20]) and/or experimentally measured [41] for the two most potent compounds **5** and **12** and the parent compound frentizole (Table 3). The obtained data were compared with optimal properties for CNS targeted drugs

[42–44]. All compounds complied with the optimal values for molecular weight, H-bond acceptors/donors, number of rotatable bonds and ClogP/ElogP values. $CLogD_{7.4}$/$ELogD_{7.4}$ values slightly diverged from the optimal range in case of **5** and **12** and all three compounds showed higher than optimal values of total polar surface area (tPSA). Regarding solubility, then only compound **5** did not fit the optimal range for the calculated $logS_{7.4}$. Generally, a good correlation between the experimental and calculated logP and $logD_{7.4}$ values was found. Taken together, the compounds **5** and **12** were predicted to penetrate the blood-brain barrier and thus might act within the CNS. However, for future structural design, it will be advantageous to improve some of the physical-chemical properties, especially the tPSA.

Table 3: Physical-chemical properties of frentizole and the most potent I nhibitors **5** and **12** compared to optimal values for CNS targeted drugs [42–44].

Compound	Mw	H-bond acceptor/donor	Rot. bonds	tPSA (Å^2)	ClogP	ELogP±SD	$ClogD_{7.4}$	$ELogD_{7.4}$ ± SD	$ClogS_{7.4}$
Optimum	≤450	≤7/≤3	<8	≤(60-70)	1-5	1-5	0-3	0-3	>(-4.5)
frentizole	299.35	5/2	3	91.49	3.2	nd	2.5	nd	-3.7
5	303.38	3/2	4	97.28	3.5	4.1 ± 0.4%o	3.5	4.1 ± 1.2%o	-4.6
12	328.39	6/3	6	107.50	3.3	3.4 ± 0.5%o	3.2	3.4 ± 0.1%o	-3.6

* nd = not determined

QSAR analyses employing MLR and a systematic variable selection algorithm provided statistically significant and robust model for prediction of the ABAD/ 17 β -HSD10 inhibition at the inhibitor concentration of 25 mM. In Table 4, the selected molecular descriptors, regression coefficients b, standard deviations of regression coefficients (STD(b)), Student's t's, and coefficients of determination V^2 for prediction of the variable by the others variables in the model. According to Student's t's, all the selected molecular descriptors are statistically significant, although relatively high values of V^2 reveal considerable inter-correlation between the predictors Mv, JGI6 and Vs.

Table 4: Description of the best MLR QSAR model for compounds **1-15** and their inhibition activities towards ABAD/ 17β-HSD10.

$$Inhibition\ (25mM) = \sum_{i=1}^{4} b_i \cdot variable$$

Variable	b	STD(b)	Student's t	V^2
Constant	1432.8	127.29	11.256	-
Mv	-1537.3	153.08	-10.042	0.6124
JGI6	-41280	2973	-13.885	0.8795

Vs	2.537	0.18438	13.759	0.8130

Statistical criteria for the best three parametric MLR QSAR model found, such as coefficient of determination R^2, Fisher-Snedecor F, standard residual deviation s, adjusted coefficient of determination R^2_{adj}, adjusted Fisher-Snedecor *FIT*, and cross-validated coefficient of determinations by leave-one-out Q^2_{LOO} and leave-30%-out $Q^2_{LMO-30\%}$ techniques, are summarized in Table 5. $_{Q2LMO-30\%}$ values were determined as a mean value of 1000 repetitions of random selection of 30% compounds from the complete set of **1-15**. The relationship between the real and predicted inhibition potencies of the compounds is outlined in Fig. 6.

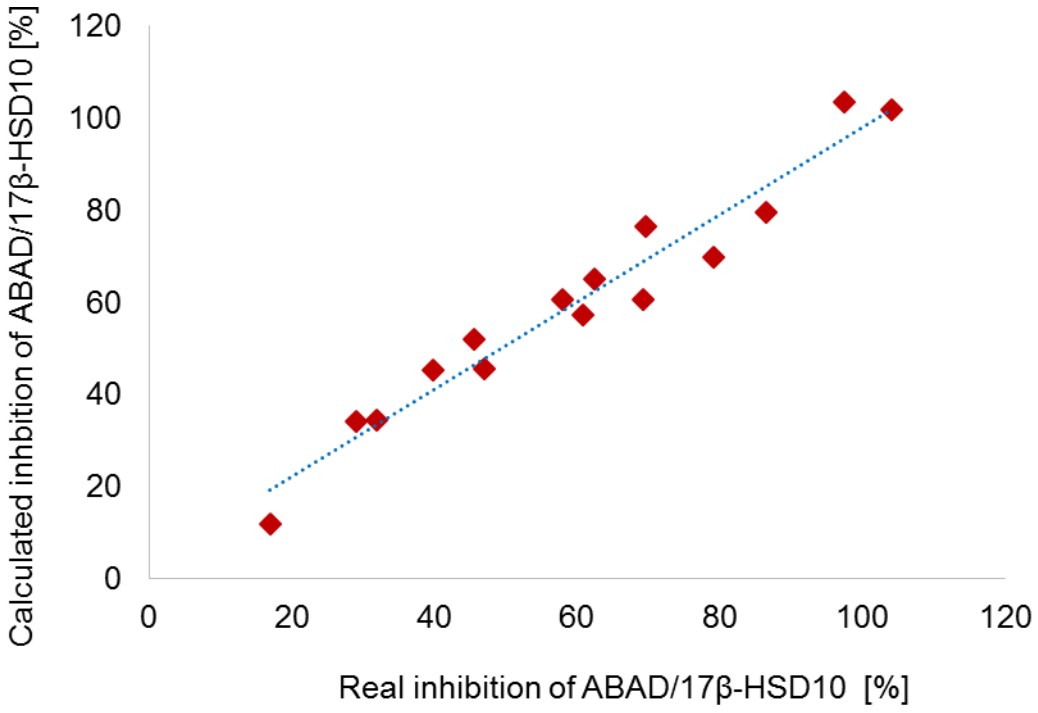

Figure 6: Real and calculated inhibition potencies of compounds **1-15** by the best MLR QSAR model.

Besides cross-validations of the best QSAR model, we also evaluated the model performance after replacement of the y vector of inhibition potencies by random variables with normal distribution (i.e. randomized y) or by its random permutation (i.e. scrambled y). Since randomization and scrambling might provide a vector with similar values to the original vector, coefficients of determination for the altered and real biological activities are mentioned as $R^2_{r/o}$ and $R^2_{s/o}$ in Table 5. High values of R^2 and F confirm that the QSAR model is internally predictive and statistically significant. Robustness of the model is proved by very high values of cross-validated coefficients of determination

Q^2_{LOO} and $Q^2_{LMO\text{-}30\%}$. Drop of all these statistical criteria after randomization and scrambling further confirms that the QSAR model is capable to discriminate chance factors in the input. However, the QSAR model was built on 15 compound and a pool of several thousand molecular descriptors, and, thus, it has to be taken with caution.

Table 5: Statistical criteria for the best MLR QSAR model representing compounds **1-15** and their inhibition activities towards ABAD/ 17β-HSD10.

QSAR Model	R^2	F	s	R^2_{adj}	FIT	Q^2_{LOO}	$Q^2_{LMO\text{-}30\%}$
Final model	0.9485	67.48	6.4933	0.9344	8.4349	0.9000	0.7609
Randomized y ($R^2_{r/o}$ = 0.0027)	0.3871	2.31	13.547	0.2199	0.2895	-0.3981	-1.6992
Scrambled y ($R^2_{s/o}$ = 0.0026)	0.2514	1.23	24.748	0.0471	0.1539	-0.4039	-1.9696

The domain of applicability of the best QSAR model was demonstrated by William's plot, which displays possible outliers in a conjugate chemical space of the biological activities and the selected molecular descriptors (Fig. 7). Only compound **12**, which exhibited the strongest inhibition activity for ABAD/ 17β-HSD10, is relatively distant from the main cluster of compounds. In general, the QSAR model is well representative for the solved problem.

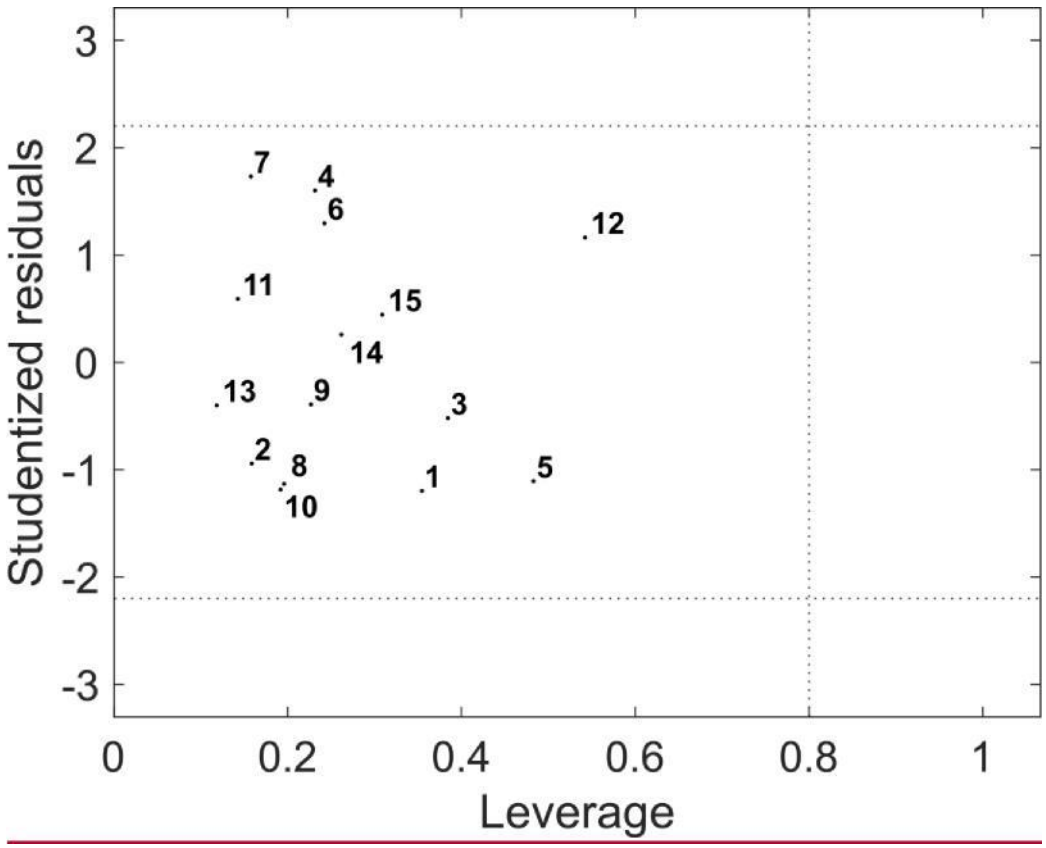

Figure 7: William's plot representing compounds **1-15** in a projection of the chemical space delimited by the MLR QSAR model. No compounds studied exhibit significant outlying, which confirms suitability of the model definition.

The above-mentioned statistical validations clearly showed that the developed MLR QSAR model is significant, robust and applicable for ABAD/17β-HSD10 inhibition predictions. The model is built only of three variables: Mv - mean atomic van der Waals volume scaled on carbon atom, JGI6 - mean topological charge index of order 6, and Vs - V total size index weighted by I-state, which enables relatively simple interpretation. If Mv is higher, the observed inhibition potency for ABAD/17β-HSD10 is stronger. This feature may be implied if the carbonyl group is replaced by thiocarbonyl or imino functions. JGI6 descriptor expresses the total charge transfer between atoms at topological distance of 6, and, thus, it is closely related with substitutions at peripheral molecular sites and molecular polarity. The higher the charge transfer (i.e. JGI6), the stronger inhibition of ABAD/17β-HSD10 is elicited. JGI6 descriptor achieves maximal values for compounds **7-12**, which are substituted with two 4-methoxy or one 4-ethyl carboxylate functions. On the other hand, Vs molecular descriptor, which belongs to WHIM group, should be less in order to support the inhibition activity. As Vs reflect the spatial molecular extent, a smaller molecules may induce a stronger inhibition. Nonetheless, Mv and Vs have opposite meaning which suggests that a certain optimum of atomic and total molecular size needs to be found.

Pharmacophore analysis of the studied compounds **1-15** in LigandScout 3.1 provided another insight into the relationships between the structure and activity of ABAD/17β-HSD10 inhibitors. By training on the most active substances, a pharmacophore hypothesis was derived and all the compounds were scored according to their fit to it. In Fig. 8., an alignment of compounds **5** and **12** with the proposed pharmacophore is demonstrated. Since the set of studied compounds exhibit a high degree of structural similarity, discrimination of inactive structural cores could not fully manifest in the calculations. The present pharmacophore analysis indicated practically the whole structure of compounds **5** or **12** as a pharmacophore. Discriminative power of the pharmacophore model was achieved mainly due to defining exclusion volumes, which enabled differentiation of the most active compounds (e.g. **5**, **12**, **9**) from the least active ones (e.g. **15**, **1**). Unfortunately, a robust pharmacophore-based QSAR model giving correct classification all the tested compounds **1-15** according to their inhibition potency was not achieved by this methodology.

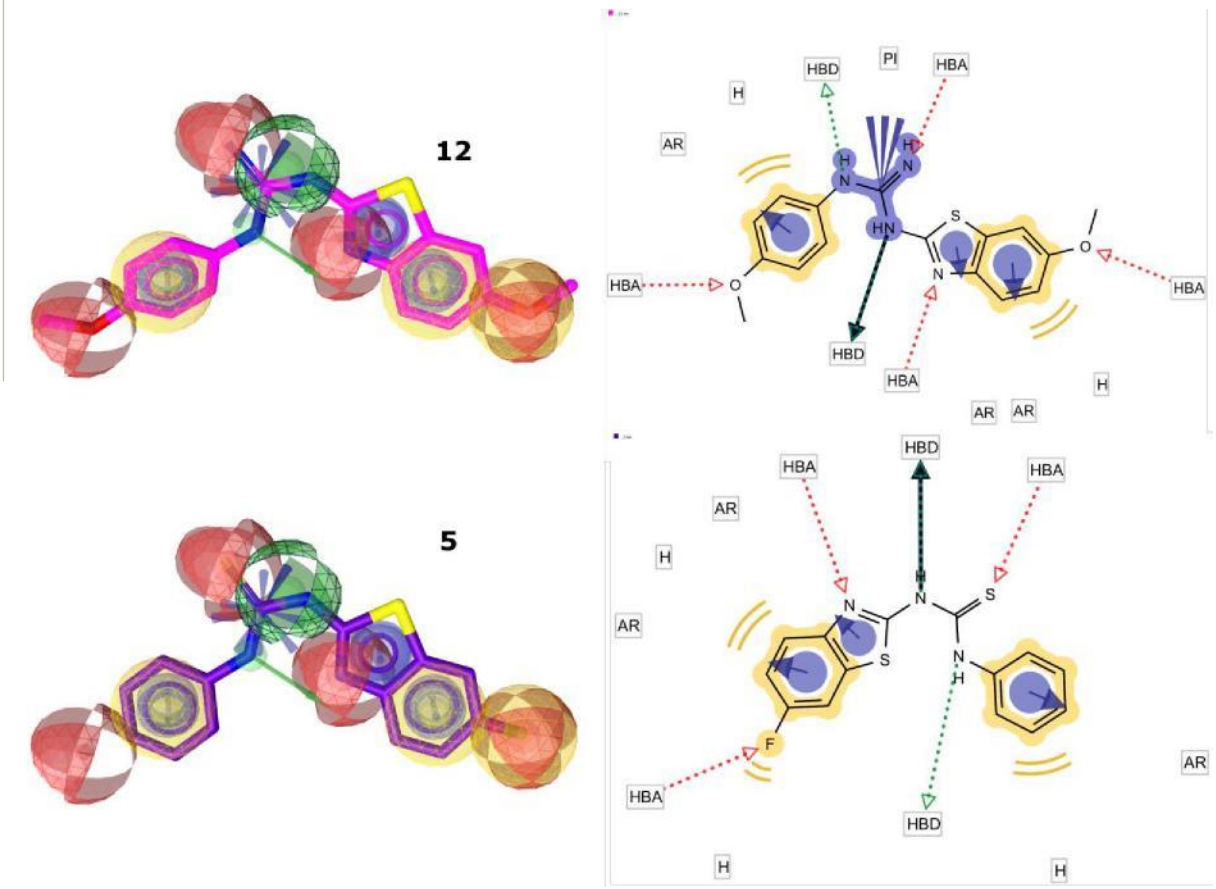

Figure 8: A pharmacophore hypothesis derived in LigandScout 3.1 with aligned compounds **5** and **12**. In the right part of the figure, proposed non-covalent interactions (HBA – hydrogen bond acceptor, HBD – hydrogen bond donor, AR – aromatic interaction, H – hydrophobic interactions, PI – positively ionisable group) of the ligands with a putative receptor are outlined.

CONCLUSION

In summary, a series of novel ABAD/ 17β-HSD10 inhibitors, analogues of frentizole, have been designed, synthesized and evaluated *in vitro*. Among the 15 prepared compounds, compound **12** was found the most promising hit with good inhibitory activity (IC50 = 3.06 ± 0.40 μM) and acceptable cytotoxicity profile comparable to the parent frentizole. Together with satisfying physical-chemical properties suggesting its capability to permeate through BBB, compound **12** presents a novel lead structure for further research and development. On the other hand, compounds encompassing the thiourea linker in their structure were found to be improper leads for further development despite their good inhibitory activity as they were suggested to act via an unspecific manner and they are possibly creating a disulphide bond with the protein's cysteine residues.

CONFLICT OF INTEREST

The authors confirm that this article content has no conflict of interest.

ACKNOWLEDGEMENTS

This work was supported by the Ministry of Health of the Czech Republic (no. NV15-28967A), by the project National Institute of Mental Health (NIMH CZ; no. ED2.1.00/03.0078)from the European Regional Development Fund, COST CA15135, The Alzheimer's Society (specifically The Barcopel Foundation) and The Biotechnology and Biological Sciences Research Council (BBSRC) (no. BB/J01446X/1).This research is part-funded by the MSD Scottish Life Sciences fund. As part of an on-going contribution to Scottish life sciences, Merck Sharp & Dohme Limited (MSD), a global healthcare leader, has given substantial monetary funding to the Scottish Funding Council (SFC) for distribution via the Scottish Universities Life Science Alliance (SULSA) to develop and deliver a high quality drug discovery research and training programme. All aspects of the programme have been geared towards attaining the highest value in terms of scientific discovery, training and impact. The opinions expressed in this research are those of the authors and do not necessarily represent those of MSD, nor its Affiliates.

REFERENCES

[1] WHO | Dementia: a public health priority http://www.who.int/mental_health/publications/dementia_report_2012/en/ (accessed May 15, **2013**).

[2] Price, D. L.; Sisodia, S. S. Mutant Genes in Familial Alzheimer's Disease and Transgenic Models. *Annu. Rev. Neurosci.* **1998**, *21*, 479–505.

[3] Selkoe, D. J. Translating Cell Biology into Therapeutic Advances in Alzheimer's Disease. *Nature* **1999**, *399* (6738 Suppl), A23-31.

[4] Hardy, J. A.; Higgins, G. A. Alzheimer's Disease: The Amyloid Cascade Hypothesis. *Science* **1992**, *256* (5054), 184–185.
[5] Dahlgren, K. N.; Manelli, A. M.; Stine, W. B., Jr; Baker, L. K.; Krafft, G. A.; LaDu, M. J. Oligomeric and Fibrillar Species of Amyloid-Beta Peptides Differentially Affect Neuronal Viability. *J. Biol. Chem.* **2002**, *277* (35), 32046–32053.
[6] Gouras, G. K.; Tsai, J.; Naslund, J.; Vincent, B.; Edgar, M.; Checler, F.; Greenfield, J. P.; Haroutunian, V.; Buxbaum, J. D.; Xu, H.; Greengard, P.; Relkin, N. R. Intraneuronal Abeta42 Accumulation in Human Brain. *Am. J. Pathol.* **2000**, *156* (1), 15–20.
[7] Wirths, O.; Multhaup, G.; Bayer, T. A. A Modified Beta-Amyloid Hypothesis: Intraneuronal Accumulation of the Beta-Amyloid Peptide--the First Step of a Fatal Cascade. *J. Neurochem.* **2004**, *91* (3), 513–520.
[8] Benek, O.; Aitken, L.; Hroch, L.; Kuca, K.; Gunn-Moore, F.; Musilek, K. A Direct Interaction between Mitochondrial Proteins and Amyloid-13 Peptide and Its Significance for the Progression and Treatment of Alzheimer`s Disease. *Curr. Med. Chem.* **2015**, *11*, 21–29.
[9] He, X. Y.; Wen, G. Y.; Merz, G.; Lin, D.; Yang, Y. Z.; Mehta, P.; Schulz, H.; Yang, S. Y. Abundant Type 10 17 Beta-Hydroxysteroid Dehydrogenase in the Hippocampus of Mouse Alzheimer's Disease Model. *Brain Res. Mol. Brain Res.* **2002**, *99* (1), 46–53.
[10] Yan, S. D.; Shi, Y.; Zhu, A.; Fu, J.; Zhu, H.; Zhu, Y.; Gibson, L.; Stern, E.; Collison, K.; Al-Mohanna, F.; Ogawa, S.; Roher, A.; Clarke, S. G.; Stern, D. M. Role of ERAB/L-3-Hydroxyacyl-Coenzyme A Dehydrogenase Type II Activity in Abeta-Induced Cytotoxicity. *J. Biol. Chem.* **1999**, *274* (4), 2145–2156.
[11] Kissinger, C. R.; Rejto, P. A.; Pelletier, L. A.; Thomson, J. A.; Showalter, R. E.; Abreo, M. A.; Agree, C. S.; Margosiak, S.; Meng, J. J.; Aust, R. M.; Vanderpool, D.; Li, B.; Tempczyk-Russell, A.; Villafranca, J. E. Crystal Structure of Human ABAD/HSD10 with a Bound Inhibitor: Implications for Design of Alzheimer's Disease Therapeutics. *J. Mol. Biol.* **2004**, *342* (3), 943–952.
[12] Lim, Y.-A.; Grimm, A.; Giese, M.; Mensah-Nyagan, A. G.; Villafranca, J. E.; Ittner, L. M.; Eckert, A.; Götz, J. Inhibition of the Mitochondrial Enzyme ABAD Restores the Amyloid-13-Mediated Deregulation of Estradiol. *PloS One* **2011**, *6* (12), e28887.
[13] Xie, Y.; Deng, S.; Chen, Z.; Yan, S.; Landry, D. W. Identification of Small-Molecule Inhibitors of the Abeta-ABAD Interaction. *Bioorg. Med. Chem. Lett.* **2006**, *16* (17), 4657–4660.
[14] Valasani, K. R.; Hu, G.; Chaney, M. O.; Yan, S. S. Structure-Based Design and Synthesis of Benzothiazole Phosphonate Analogues with Inhibitors of Human ABAD-A13 for Treatment of Alzheimer's Disease. *Chem. Biol. Drug Des.* **2013**, *81* (2), 238–249.
[15] Valasani, K. R.; Sun, Q.; Hu, G.; Li, J.; Du, F.; Guo, Y.; Carlson, E. A.; Gan, X.; Yan, S. S. Identification of Human ABAD Inhibitors for Rescuing A13-Mediated Mitochondrial Dysfunction. *Curr. Alzheimer Res.* **2014**, *11* (2), 128–136.
[16] He, X.-Y.; Wegiel, J.; Yang, Y.-Z.; Pullarkat, R.; Schulz, H.; Yang, S.-Y. Type 10 17beta-Hydroxysteroid Dehydrogenase Catalyzing the Oxidation of Steroid Modulators of Gamma-Aminobutyric Acid Type A Receptors. *Mol. Cell. Endocrinol.* **2005**, *229* (1–2), 111–117.
[17] He, X.-Y.; Yang, S.-Y. Roles of Type 10 17beta-Hydroxysteroid Dehydrogenase in Intracrinology and Metabolism of Isoleucine and Fatty Acids. *Endocr. Metab. Immune Disord. Drug Targets* **2006**, *6* (1), 95–102.
[18] Ayan, D.; Maltais, R.; Poirier, D. Identification of a 1713-Hydroxysteroid Dehydrogenase Type 10 Steroidal Inhibitor: A Tool to Investigate the Role of Type 10 in Alzheimer's Disease and Prostate Cancer. *ChemMedChem* **2012**, *7* (7), 1181–1184.
[19] Mancini, D. T.; Souza, E. F.; Caetano, M. S.; Ramalho, T. C. 99Tc NMR as a Promising Technique for Structural Investigation of Biomolecules: Theoretical Studies on the Solvent and Thermal Effects of Phenylbenzothiazole Complex. *Magn. Reson. Chem.* **2014**, *52* (4), 129–137.
[20] ACD/Labs PhysChemSuite 12.0, Advanced Chemistry Development, Inc., Toronto, On, Canada, Www.acdlabs.com, 2012.
[21] OECD. *Test No. 117: Partition Coefficient (N-Octanol/Water), HPLC Method*; OECD Publishing.
[22] Mancini, D. T.; Sen, K.; Barbatti, M.; Thiel, W.; Ramalho, T. C. Excited-State Proton Transfer Can Tune the Color of Protein Fluorescent Markers. *ChemPhysChem* **2015**, *16* (16), 3444– 3449.
[23] Aitken, L.; Quinn, S. D.; Perez-Gonzalez, C.; Samuel, I. D. W.; Penedo, J. C.; Gunn-Moore, F. J. Morphology-Specific Inhibition of 13-Amyloid Aggregates by 1713-Hydroxysteroid Dehydrogenase Type 10. *Chembiochem Eur. J. Chem. Biol.* **2016**, *17* (11), 1029–1037.

[24] Hroch, L.; Benek, O.; Guest, P.; Aitken, L.; Soukup, O.; Janockova, J.; Musil, K.; Dohnal, V.; Dolezal, R.; Kuca, K.; Smith, T. K.; Gunn-Moore, F.; Musilek, K. Design, Synthesis and in Vitro Evaluation of Benzothiazole-Based Ureas as Potential ABAD/17β-HSD10 Modulators for Alzheimer's Disease Treatment. *Bioorg. Med. Chem. Lett.* **2016**, *26* (15), 3675–3678.
[25] Kissinger, C. R.; Rejto, P. A.; Pelletier, L. A.; Thomson, J. A.; Showalter, R. E.; Abreo, M. A.; Agree, C. S.; Margosiak, S.; Meng, J. J.; Vanderpool, R.; Li, B.; Tempczyk-Russell, A.; Villafranca, J. E. Crystal Structure of Human ABAD/HSD10 with a Bound Inhibitor: Implications for Design of Alzheimer's Disease Therapeutics. *J. Mol. Biol.* **2004**, *342* (3), 943–952.
[26] HyperChem(TM) Professional 8.0, Hypercube, Inc., 1115 NW 4th Street, Gainesville, Florida 32601, USA.
[27) *Talete Srl, Dragon (Software for Molecular Descriptor Calculation), Version 6.0; **2015**.*
[28] Dolezal, R.; Waisser, K.; Petrlíková, E.; Kunes, J.; Kubicová, L.; Machácek, M.; Kaustová, J.; Dahse, H. M. N-Benzylsalicylthioamides: Highly Active Potential Antituberculotics. *Arch. Pharm. (Weinheim)* **2009**, *342* (2), 113–119.
[29] Topliss, J. G.; Edwards, R. P. Chance Factors in Studies of Quantitative Structure-Activity Relationships. *J. Med. Chem.* **1979**, *22* (10), 1238–1244.
[30] Dolezal, R.; Van Damme, S.; Bultinck, P.; Waisser, K. QSAR Analysis of Salicylamide Isosteres with the Use of Quantum Chemical Molecular Descriptors. *Eur. J. Med. Chem.* **2009**, *44* (2), 869–876.
[31] Tosco, P.; Balle, T.; Shiri, F. Open3DALIGN: An Open-Source Software Aimed at Unsupervised Ligand Alignment. *J. Comput. Aided Mol. Des.* **2011**, *25* (8), 777.
[32] Taminau, J.; Thijs, G.; De Winter, H. Pharao: Pharmacophore Alignment and Optimization. *J. Mol. Graph. Model.* **2008**, *27* (2), 161–169.
[33] Richmond, N. J.; Willett, P.; Clark, R. D. Alignment of Three-Dimensional Molecules Using an Image Recognition Algorithm. *J. Mol. Graph. Model.* **2004**, *23* (2), 199–209.
[34] Dolezal, R.; Korabecny, J.; Malinak, D.; Honegr, J.; Musilek, K.; Kuca, K. Ligand-Based 3D QSAR Analysis of Reactivation Potency of Mono- and Bis-Pyridinium Aldoximes toward VX-Inhibited Rat Acetylcholinesterase. *J. Mol. Graph. Model.* **2015**, *56*, 113–129.
[35] Bernas, T.; Dobrucki, J. Mitochondrial and Nonmitochondrial Reduction of MTT: Interaction of MTT with TMRE, JC-1, and NAO Mitochondrial Fluorescent Probes. *Cytometry* **2002**, *47* (4), 236–242.
[36] Abe, K.; Matsuki, N. Measurement of Cellular 3-(4,5-Dimethylthiazol-2-Yl)-2,5-Diphenyltetrazolium Bromide (MTT) Reduction Activity and Lactate Dehydrogenase Release Using MTT. *Neurosci. Res.* **2000**, *38* (4), 325–329.
[37] Malinak, D.; Dolezal, R.; Marek, J.; Salajkova, S.; Soukup, O.; Vejsova, M.; Korabecny, J.; Honegr, J.; Penhaker, M.; Musilek, K.; Kuca, K. 6-Hydroxyquinolinium Salts Differing in the Length of Alkyl Side-Chain: Synthesis and Antimicrobial Activity. *Bioorg. Med. Chem. Lett.* **2014**, *24* (22), 5238–5241.
[38] Hroch, L.; Aitken, L.; Benek, O.; Dolezal, M.; Kuca, K.; Gunn-Moore, F.; Musilek, K. Benzothiazoles - Scaffold of Interest for CNS Targeted Drugs. *Curr. Med. Chem.* **2015**, *22* (6), 730–747.
[39] Furlan, A.; Colombo, F.; Kover, A.; Issaly, N.; Tintori, C.; Angeli, L.; Leroux, V.; Letard, S.; Amat, M.; Asses, Y.; Maigret, B.; Dubreuil, P.; Botta, M.; Dono, R.; Bosch, J.; Piccolo, O.; Passarella, D.; Maina, F. Identification of New Aminoacid Amides Containing the imidazo[2,1-B]benzothiazol-2-Ylphenyl Moiety as Inhibitors of Tumorigenesis by Oncogenic Met Signaling. *Eur. J. Med. Chem.* **2012**, *47*, 239–254.
[40] van Montfort, R. L. M.; Congreve, M.; Tisi, D.; Carr, R.; Jhoti, H. Oxidation State of the Active-Site Cysteine in Protein Tyrosine Phosphatase 1B. *Nature* **2003**, *423* (6941), 773–777.
[41] OECD. *Test No. 117: Partition Coefficient (N-Octanol/Water), HPLC Method*; OECD Guidelines for the Testing of Chemicals, Section 1; OECD Publishing, 2004.
[42] Pajouhesh, H.; Lenz, G. R. Medicinal Chemical Properties of Successful Central Nervous System Drugs. *NeuroRx J. Am. Soc. Exp. Neurother.* **2005**, *2* (4), 541–553.
[43] Wenlock, M. C.; Austin, R. P.; Barton, P.; Davis, A. M.; Leeson, P. D. A Comparison of Physiochemical Property Profiles of Development and Marketed Oral Drugs. *J. Med. Chem.* **2003**, *46* (7), 1250–1256.
[44] Alelyunas, Y. W.; Empfield, J. R.; McCarthy, D.; Spreen, R. C.; Bui, K.; Pelosi-Kilby, L.; Shen, C. Experimental Solubility Profiling of Marketed CNS Drugs, Exploring Solubility Limit of CNS Discovery Candidate. *Bioorg. Med. Chem. Lett.* **2010**, *20* (24), 7312–7316.